UNIVERSITY OF CALIFORNIA SAN DIEGO

An Unsupervised Approach for Predicting Transporter-Mediated Drug-Metabolite Interactions

A thesis submitted in partial satisfaction of the requirements for the degree Master of Science

in

Biology

by

Julia G. Li

Committee in charge:

Professor Sanjay Nigam, Chair
Professor Milton Saier, Co-Chair
Professor Julian Schroeder

2020

The thesis of Julia G. Li is approved, and it is acceptable in quality and form for publication on microfilm and electronically.

University of California San Diego

2020

TABLE OF CONTENTS

LIST OF ABBREVIATIONS

1D	One-dimensional
2D	Two-dimensional
5-CF	5-Carboxyfluorescein
6-CF	6-Carboxyfluorescein
AHR	Aryl hydrocarbon receptor
CCC	Cophenetic correlation coefficient
CKD	Chronic kidney disease
CMPF	3-Carboxy-4-methyl-5-propyl-2-furanpropionate
CVD	Cardiovascular disease
Cys	Cysteine
DB	Davies-Bouldin
DDI	Drug-drug interaction
DME	Drug-metabolizing enzyme
DMI	Drug-metabolite interaction
FDA	Food and Drug Administration
FP	Fingerprint
FXR	Farsenoid X receptor
GPCR	G protein-coupled receptor
HAC	Hierarchical agglomerative clustering
HEK	Human embryonic kidney
IC_{50}	Half-maximal inhibitory concentration
ICM	Internal Coordinate Mechanics
Ile	Isoleucine
KDE	Kernel density estimate

K_i	Inhibition constant
K_m	Michaelis constant
KO	Knockout
Leu	Leucine
MTX	Methotrexate
NSAIDs	Nonsteroidal anti-inflammatory drugs
OAT	Organic anion transporter
OATP	Organic anion transporting polypeptide
PC	Principal component
PCA	Principal component analysis
Phe	Phenylalanine
PT	Proximal tubule
SLC	Solute carrier
SMILES	Simplified Molecular Input Line Entry System
Tc	Tanimoto coefficient
TGR5	G protein-coupled bile acid receptor 1; GPBAR1
Trp	Tryptophan
TS	Threshold similarity
Tyr	Tyrosine
U/D	Unpublished data
WCSS	Within-cluster sum of squares

LIST OF SUPPLEMENTAL FILES

li_01_oat1_chemical_dataset_smiles.csv

li_02_oat3_chemical_dataset_smiles.csv

li_03_in_vitro_oat1_metabolite_smiles.csv

li_04_in_vitro_oat3_metabolite_smiles.csv

li_05_ccc_outputs.xlsx

li_06_high_confidence_dmis.xlsx

li_07_workflow.pdf

LIST OF FIGURES

LIST OF TABLES

ACKNOWLEDGEMENTS

I would like to express my sincere gratitude to my advisor Dr. Sanjay Nigam for the steadfast support of my research, for his patience, enthusiasm and guidance. He has been an invaluable resource and an exceptional mentor during the two and a half years that I worked in the Nigam Lab. I am extremely thankful to Dr. Milton Saier and Dr. Julian Schroeder for their encouragement, insightful comments and constructive feedback on my project.

I want to give special thanks to Da Shi for his guidance in computational chemistry during my early days in the computer lab. His support has prompted me to widen my research from a data-driven perspective. I would also like to thank Dr. Ruben Abagyan, who gave me access to their computer lab and his lab's expertise to pursue this research.

I thank all my fellow lab mates for their friendship and a cherished time spent together in the Nigam Lab. In particular, I am grateful to Jeffry Granados for being constantly available for scientific discussion.

I have been so fortunate to have had many incredible collaborators and mentors throughout my time in the Nigam Lab and I am grateful to every person who has supported me and contributed to my research process.

ABSTRACT OF THE THESIS

An Unsupervised Approach for Predicting Transporter-Mediated Drug-Metabolite Interactions

by

Julia G. Li

Master of Science in Biology

University of California San Diego, 2020

Professor Sanjay Nigam, Chair
Professor Milton Saier, Co-Chair

Organic anion transporter 1 (OAT1) and 3 (OAT3) are multi-specific renal drug transporters that facilitate the uptake and clearance of a wide range of endogenous and exogenous molecules. While they've been extensively studied for their clinical role in drug disposition and potential drug-drug interactions (DDIs), their physiological role in regulating

metabolism and systemic homeostasis is less understood. With the availability of new metabolomics data, we explore drug-metabolite interactions (DMIs) and their potential impacts on metabolic pathways through the use of chemical spaces presented herein and challenge the well established *in silico* virtual screening approach formulated under the assumption that structural similarity is necessary for a potential DDI. Overall, our analyses help elucidate the role of OAT-mediated drug-metabolite interactions in drug-induced metabolic dysregulation and provide insight into the unexplained side effects and toxicities from long-term drug treatment and/or polypharmacotherapy.

INTRODUCTION

Organic anion transporters, or OATs, are 12-transmembrane domain proteins that are classified within the SLC (solute carrier) superfamily. They are expressed in barrier epithelia including the renal proximal tubules (PTs), liver, choroid plexus, olfactory mucosa, brain, retina and placenta (S. K. Nigam et al., 2015). They play a cooperative role in mediating the absorption and excretion of a variety of small organic anionic molecules (Roth et al., 2012). While OATs are well-studied due to their pharmacological importance for drug disposition, they also play a central role in systemic physiology and remote inter-organ and inter-organismal communication by regulating circulating levels of endogenous signaling molecules and key metabolites between tissues, body fluids and different organisms, as described by the "Remote Sensing and Signaling Theory" (S. K. Nigam, 2014).

OAT1 (SLC22A6) and OAT3 (SLC22A8), which are abundantly expressed on the basolateral side of the renal PT epithelial cells, represent the key rate-limiting step for the renal elimination of a wide range of endogenous (e.g., prostaglandins, cyclic nucleotides, fatty acids, bile acids, signaling molecules, TCA intermediates, uremic toxins) and exogenous (e.g., drugs, natural products, environmental toxins, hepatic phase I/II DME-derived products) organic anion molecules. In fact, they are the most widely studied members of the OAT group due to their pharmaceutical relevance. At the active drug secretion site, OAT1 and OAT3 interact with a wide range of drugs, such as diuretics, cephalosporins, chemotherapeutics, antihypertensives, antivirals and nonsteroidal anti-inflammatory drugs (NSAIDs). The FDA has recently recommended that novel drug entities be screened against 7 drug transporters, including OAT1 and OAT3, due to the possibility of drug-drug interactions, where two or more drugs compete for the same transporter (Giacomini et al., 2010). DDIs at the OAT-level as a result of combination

therapy can significantly alter drug clearance from the blood and consequently, cause unexpected drug side effects and toxicities. For example, combined treatment of NSAIDs, such as diclofenac, ibuprofen, naproxen and flurbiprofen, with the chemotherapeutic methotrexate (MTX) leads to reduced MTX clearance. The inhibitory effects of NSAIDs on OAT-mediated renal clearance of MTX leads to greater systemic exposure of MTX, which increases the risk of drug-induced toxicity and adverse drug effects such as hemodynamic changes, kidney injury, liver impairment and gastrointestinal disorders (Iwaki et al., 2017). If such clinical DDIs are not accounted for in drug dosing, they can have harmful, even fatal clinical consequences.

While they are commonly referred to as "drug" transporters due to their large number of drug substrates, OAT1 and OAT3 also interact with a wide range of endogenous organic anion compounds and play an important physiological role in the regulation of key metabolic pathways and levels of signaling molecules, as well as gut microbiome-derived uremic toxins. OAT3 in particular may play a larger role in systemic metabolism by regulating the flow of metabolites through the gut-liver-kidney axis, while OAT1 may be more important in regulating local kidney PT energy metabolism (Bush et al., 2017).

Recent metabolomics studies in *Oat1KO*, *Oat3KO* and "chemical double" knockout (*Oat3KO* and probenecid) mice help illustrate the independent and synergistic roles of OAT1 and OAT3 in regulating uremic metabolism. Uremic toxins, or uremic retention solutes, represent a diverse set of endogenous small molecules that are normally cleared via renal excretion in healthy patients but are elevated in the plasma of patients with renal impairment. OAT1 and OAT3 facilitate the uptake and renal clearance of many of these uremic compounds, including those derived from the gut microbiome (e.g., indoxyl sulfate, CMPF, phenyl sulfate, indoleacetate), from the blood into the urine. While several appear to be substrates for both

OATs (e.g., p-cresol sulfate), certain uremic toxins, such as CMPF and trimethylamine N-oxide (TMAO), seem to prefer OAT3, while kynurenine, kynurenate, hypoxanthine and orotate are more likely to interact with OAT1 (Wu et al., 2017).

Uremic syndrome, characterized by the accumulation of uremic solutes in the plasma, is associated with multiple disorders, including chronic kidney disease (CKD), metabolic syndrome, hyperlipidemia, cardiovascular disease, diabetes and other disorders. One explanation for off-target drug effects, especially in the context of long-term drug treatment and comorbidities, such as CVD and diabetes, is that they compete with uremic toxins for OAT-mediated renal clearance, thereby increasing uremic toxin concentrations in the plasma. For example, combined intake of NSAIDs, such as ketoprofen and diclofenac, and co-administration of antihypertensive can impair OAT-mediated renal clearance of indoxyl sulfate, resulting in greater systemic exposure of indoxyl sulfate and risk of drug-induced toxicity and adverse effects, including CKD progression and CVD mortality (Kaminski et al., 2019; Yu et al., 2017). Other studies have also implicated NSAIDs as causes of acute renal failure, especially in elderly patients with comorbidities and drug combinations (e.g., angiotensin-converting enzyme inhibitors, angiotensin II receptor blockers, beta blockers, diuretics) (Hörl, 2010). Such interactions between NSAIDs, antihypertensive agents and uremic toxins are clinically important and thus need to be considered in dosing, especially in polypharmacotherapy.

Work by our group and others has determined that drug transporters are active in far more than just drug handling. Uncovering the endogenous role of drug transporters could have a major impact on our understanding of small-molecule drug side effects. Structurally unique drugs of various classes with different mechanisms of action can all potentially result in similar side effects. Thus, it is possible that metabolic perturbations from inhibition of multi-specific

drug transporters could contribute to this. The nature of some transported metabolites as signaling molecules also suggests that the inhibition of drug transporters can impact intracellular signaling, which may also lead to negative consequences. We focused on renal drug transporters OAT1 and OAT3, which have been extensively analyzed from both a pharmaceutical and physiological perspective, to predict potential drug-metabolite interactions.

Drug-metabolite interactions have received little research interest, but they may have a major role in how we understand the disruption of endogenous metabolism. To explore this possibility in the context of drug transporters, we first compiled lists of metabolites/drugs known to interact with OAT1 and OAT3. We then explored the similarities between the drug and metabolite spaces through the use of 1D molecular descriptors and Morgan fingerprints. Using unsupervised learning techniques, we were able to cluster the data into groups that contained both drugs and metabolites. In doing so, we obtained structurally related groups of molecules predicted to compete for the same transporter substrate binding site. These drug-metabolite pairings were then ranked by confidence. Interestingly, we found that for these transporters, physicochemical similarity was not necessary for a potential DMI. This was supported by existing knowledge of drug-drug interactions.

MATERIALS AND METHODS

Data Collection

A list of *in vitro* drugs and endogenous metabolites significantly elevated in the plasma of probenecid-treated rodents (*in vivo* metabolites) was prepared for each OAT isoform. We collected 97 *in vitro* drugs for OAT1 and 109 for OAT3 via an extensive literature search and 117 endogenous metabolites significantly elevated in the plasma of probenecid-treated rodents (n=3 for both mice and rodents). Animal handling procedures and metabolomics analyses were performed as previously described (Wu et al., 2017). Welch's two-tailed t-test (probenecid-treated vs. wild type) was used for statistical comparisons, with a p-value≤0.10 indicating statistical significance.

Calculate 1D Molecular Descriptors

The 2D chemical structures were imported to the computational environment of the commercially available cheminformatics suite ICM Chemist (Molsoft, LLC) and standardized (remove salts and explicit hydrogens, standardize chemical groups). Once standardized, they were converted to SMILES (Simplified Molecular Input Line Entry System) strings and a list of 77 1D molecular descriptors were calculated as previously described (A. K. Nigam et al., 2020). Complexity values were obtained from PubChem. A categorical variable was created to indicate compound type: 'drug', 'metabolite' or 'both' and added to the compound dataset.

Data Cleaning and Preprocessing

The compound dataset of 1D descriptors was input into Jupyter (IPython) Notebook and assessed for inconsistent values. We used the data structures and data manipulation tools provided by the Pandas and NumPy Python libraries. The 'pKa_mb' feature had object type values and was thus removed from the dataset. The remaining continuous features were centered

and scaled to unit variance with the `StandardScaler` function from scikit-learn. Categorical features were replaced with numerical values: '0' for metabolite, '1' for drug and '2' for 'both' compounds.

Feature Reduction with PCA

Scikit-learn's principal component analysis algorithm `PCA` was applied to the scaled (original) data to eliminate redundancy and reduce the dimensionality of the dataset. The original data was projected to a low dimensional space using principal components (PCs). The Matplotlib and seaborn data visualization libraries were used to generate graphics and plots. A total variance threshold of 90% was set to ensure that the transformed (PCA reduced) data is reflective of the original high dimensional data.

Decomposition Step 1: K-Means Clustering

Scikit-learn's K-means algorithm `KMeans` was fit to the reduced data, with the pre-specified parameters of random seed `(random_state=0)` and number of desired clusters `(n_clusters)`. For a range of clusters k from 2 to 10, the silhouette method was used to evaluate the performance (goodness of fit) of the model and determine the optimal number of clusters to partition the compound dataset into. The elbow method and Davies-Boulding (DB) method were used to validate the findings by the silhouette method. Once the compound dataset was partitioned by `KMeans`, we recovered the drugs and metabolites from the cluster with probenecid.

a. Silhouette Method

For each instance i, the silhouette score $s(i)$ is computed as follows:

$$s(i) = \frac{b(i) - a(i)}{\max\{a(i), b(i)\}}$$

where $b(i)$ is the mean distance between i and all other intra-cluster instances and $a(i)$ is the minimum average distance between i and all the instances in neighboring clusters.

b. *Elbow Method*

The within-cluster sum of squares (WCSS), or inertia, for each k value is plotted and visualized in a line plot. The optimal number of clusters is found at the 'elbow' of the graph (i.e., the point after which intra-cluster variance start decreasing in a linear manner).

c. *Davies-Boudin Method*

The Davies-Boudin method aims to maximize both inter-cluster (between-cluster) separation as well as intra-cluster (within-cluster) homogeneity. For each number of clusters C_k, the Davies-Bouldin index DB is calculated as follows:

$$DB(C_k) = \frac{1}{k}\sum_{i=1}^{k} \max_{i \neq j} D_i$$

where D_i is the ratio between the average intra-cluster distances $S_i + S_j$ and inter-cluster distances D_{ij} for clusters i and j. D_i is defined as:

$$D_i = \frac{S_i + S_j}{D_{ij}}$$

Construction of the Tanimoto Similarity Matrix

The chemical dataset of SMILES strings was input into Jupyter Notebook and converted to 2D structures. Morgan circular fingerprints (with radius 2 and bit length 2048) were generated for each compound. The RDKit cheminformatics package was used to analyze, manipulate and plot molecules and generate binary (2D) fingerprints. The Tanimoto/Jaccard metric was used to compute all pairwise molecular similarities and construct the similarity matrix. For two molecules/fingerprints A and B, the Tanimoto coefficient Tc_{AB} is calculated as follows:

$$Tc_{AB} = \frac{N_{A\&B}}{N_A + N_B - N_{A\&B}}$$

where N_A is the number of bits in molecule A, N_B is the number of bits in molecule B and $N_{A\&B}$ is the number of bits (structural features) common to both fingerprints A and B.

Decomposition Step 2: Hierarchical Agglomerative Clustering

The HAC algorithm `fcluster` from SciPy was used to group compounds in a bottom-up manner based on Morgan FP similarity. We determined the best linkage method for hierarchical clustering using the cophenetic correlation coefficient (CCC). The cut-off distance d for optimal number of clusters was determined using the dendrogram tree diagram and a variant of the elbow method (second derivative method). Drugs and metabolites within the probenecid cluster were obtained.

Decomposition Step 3: Co-Clustering Method

The drugs and metabolites overlapping ('co-clustering') between the probenecid-containing K-Means and hierarchical clusters (i.e., subsets of molecules obtained from the first two decomposition steps) were identified and recovered.

OAT-Mediated DMI Predictions

A list of in *vitro* metabolites, 99 for OAT1 and 76 for OAT3, was compiled from literature and used to identify which of the co-clustering metabolites are validated to be endogenous substrates *in vitro*. The *in vitro* validated metabolites are predicted to be involved in clinically relevant DMIs with the co-clustering drugs at the transporter level. Pairwise similarity scores between the co-clustering drugs and *in vitro* validated metabolites were computed using the Tanimoto metric and Morgan FPs. The score at the 90th percentile was set as the threshold (90% TS) for high confidence DMI predictions.

Inhibition of Fluorescent Tracer Uptake by Metabolite Compounds

In vitro transporter assays were run in quintuplicate (n=5) on the same plate to investigate the concentration-dependent inhibition of fluorescent tracer uptake (6-CF for OAT1; 5-CF for OAT3) by metabolite compounds (0 to 1 mM) in HEK293 cells stably overexpressing the transporter. Fluorescence was measured 10 minutes after exposure. Parallel experiments were run in triplicate (n=3) on the same plate using probenecid as a negative control. Half-maximal inhibitory concentration (IC_{50}) was calculated from curve fitting using nonlinear regression in GraphPad Prism (version 9). Transporter kinetics (K_m or K_i/IC_{50} values) for untested metabolite compounds were obtained from literature data.

Validate Clinical DDIs

DDI predictions between probenecid and the co-clustering drugs were validated via the Drug Interactions Checker tool (Drugs.com, 2020; Medscape, 2020) and literature data. Mean and median similarity scores between the probenecid-drug pairs and probenecid-metabolite pairs were computed and compared.

RESULTS

1. OAT1

Summary

Here, we utilize two different input descriptor spaces (1D molecular descriptors and 2D circular fingerprints) and partitioning methods (K-Means and average linkage hierarchical clustering) to obtain an optimized subset of structurally related molecules predicted to compete for the same substrate binding site of OAT1. We identify the following OAT1-mediated metabolic pathways affected by DMIs: amino acid metabolism (Tyr, Trp, Leu, Ile, Cys and Phe metabolism), fatty acid metabolism and vitamin B6 metabolism. Kynurenate, kynurenine and cysteine are prototype protein-bound uremic toxins predicted to have their levels elevated in the plasma due to competition for OAT1-mediated renal elimination. The competing drug compounds belong to the following therapeutic classes: analgesics, renal protectants, uricosurics, antibiotics, NSAIDs, mucolytics, antihypertensives, antidiabetics, chemotherapeutics, antivirals and diuretics. We predict that the administration of one or a combination of these drugs can cause metabolic alterations (of all these metabolites) and unexpected side effects in patients.

Decomposition Step 1: K-Means Clustering

Figure 1.1 shows that the first 15 principal components explain 90.2% of the total variance and are thus retained in the transformed compound dataset. In Figure 1.2A, the mean silhouette score is highest at k=3, thus indicating 3 to be the optimal number of clusters to partition the data into. The silhouette plots in Figure 1.2B allow for visualization of cluster assignments and distribution of individual scores for k=3 and indicate the following: the clusters are relatively homogenous in size and the probenecid cluster has a majority of its instances with

silhouette scores greater than the mean and an insignificant number that are clustered incorrectly (in the negatives).

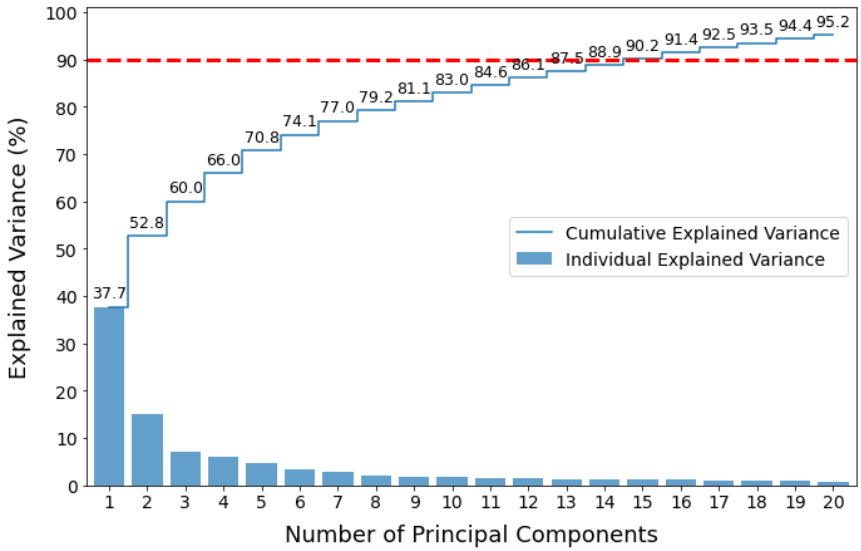

Figure 1. 1: PCA scree plot. Bar graph with individual explained variance and step chart with cumulative explained variance vs. principal components. Red-dashed line represents the 90% cumulative variance threshold.

The elbow plot in Figure 1.2C shows the elbow to be located between k=3 and k=4. After this point, intra-cluster variability decreases less rapidly with each additional cluster k. Inter-cluster separation and intra-cluster similarity is maximum at k=3 as shown in Figure 1.2D. The three evaluation methods are in agreement; k=3 partitions the compound dataset such that the resulting clusters are distinct, dense and homogenous cluster and is thus optimal for K-Means clustering. The compound dataset is decomposed to a subset of 118 structurally related molecules based on 1D molecular descriptors. 72 endogenous metabolites and 46 drugs, including probenecid, are recovered from cluster 3. The remaining 46% (102/220) of the chemical dataset is discarded.

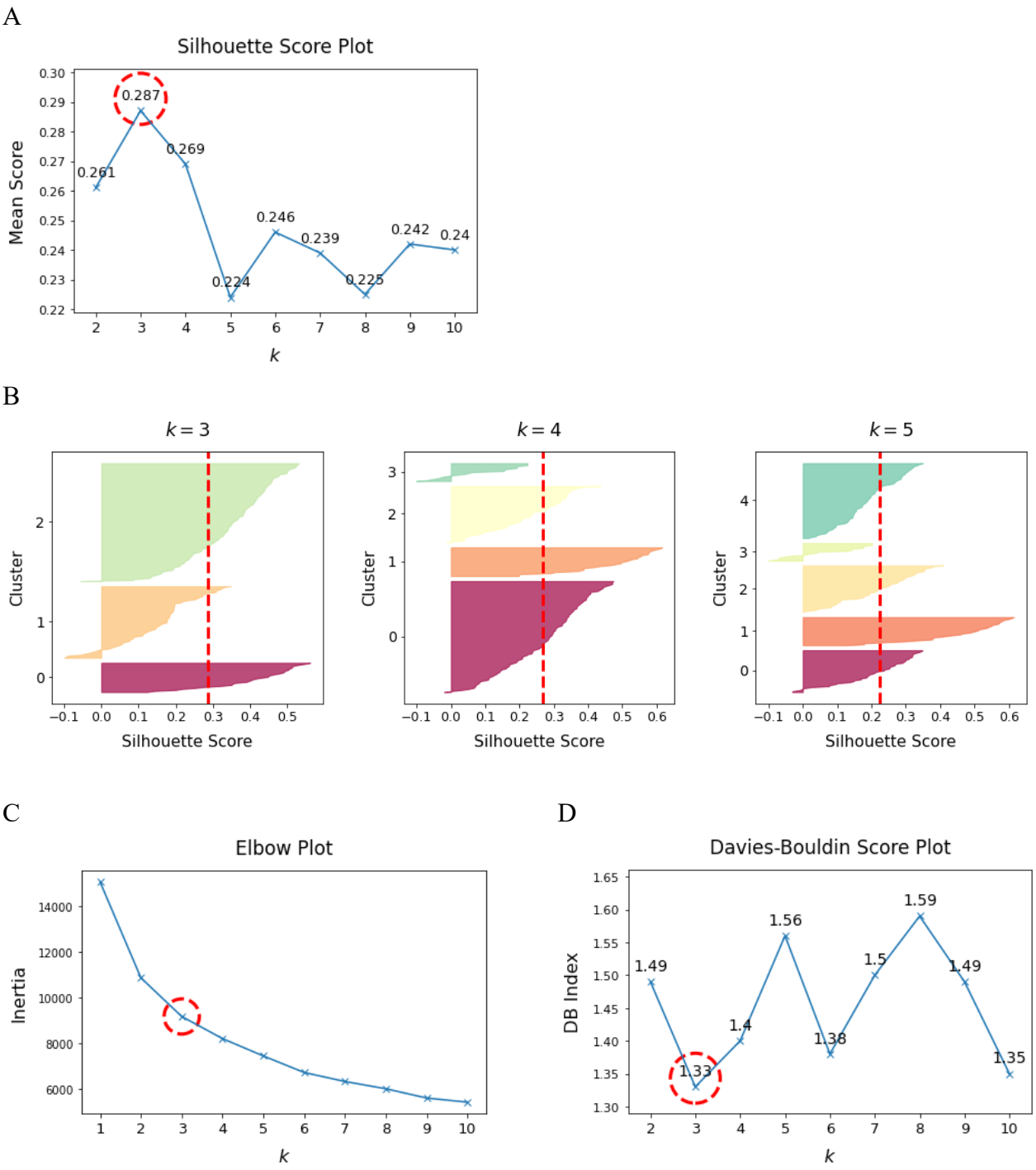

Figure 1. 2: Evaluation results on the internal evaluation of `KMeans`. The optimal score for each parameter – (A) silhouette, (C) elbow or (D) Davies-Bouldin – is circled in red. (B) Height of the silhouette plot indicates cluster size. Widths correspond to individual silhouette scores. Red-dashed vertical lines represent mean silhouette scores.

Decomposition Step 2: Hierarchical Agglomerative Clustering

Average linkage has the highest CCC (0.862) and is thus the optimal method for hierarchical clustering (li_05_ccc_outputs.xlsx). In other words, average linkage hierarchical clustering preserves the "ground truth" similarities, defined by the Tanimoto metric, between molecules the best. The dendrogram tree denotes significant jumps between the first two cluster splits and the next two splits (0.48 and 0.27, respectively). At these distance thresholds, we obtain two and three clusters, respectively, with optimized (high) inter-cluster dissimilarity. The absolute second derivative is maximum at k=3 as shown in Figure 1.3B. Thus, a cut-off distance of d=2.2 was set to partition the chemical dataset into three optimal clusters based on Morgan FPs. 73 endogenous metabolites and 101 drugs, including probenecid, are recovered from cluster 1. The remaining 21% (46/220) of the chemical dataset is discarded.

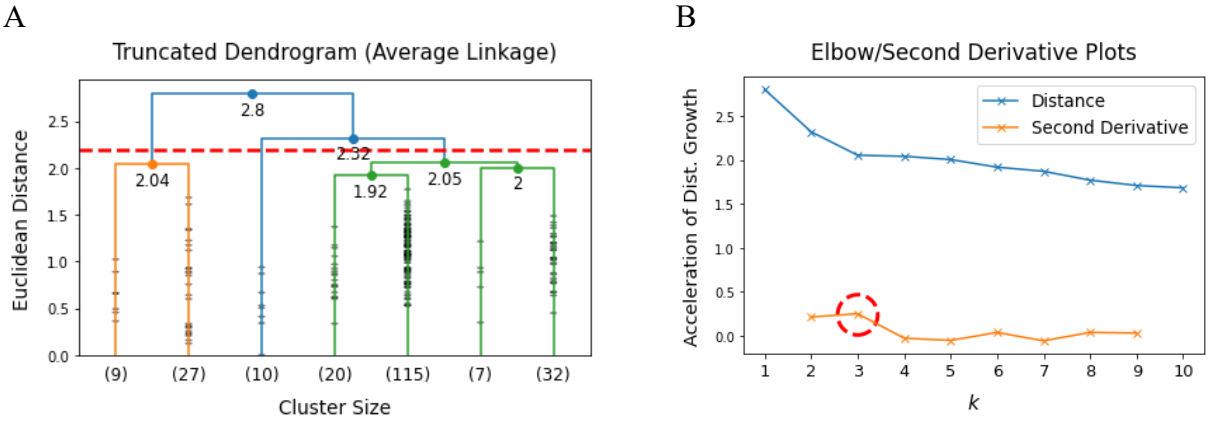

Figure 1. 3: Average linkage hierarchical clustering results. Red-dashed line indicates the cut-off distance. Red circle represents the maximum absolute second derivative, which corresponds to the elbow on the blue curve. (B) Second derivative values measure the rates at which the distances between clustering steps change.

Decomposition Step 3: Co-Clustering Method

68 metabolites and 46 drugs overlap ('co-cluster') between the probenecid-containing K-Means and hierarchical clusters. As such, the co-clustering method further decomposes the

chemical dataset to a subset of 114 compounds that have been optimized for molecular similarity using two different molecular representations and clustering algorithms.

OAT1-Mediated DMI Predictions

Out of the 68 co-clustering *in vivo* metabolites (significantly elevated in the plasma of probenecid-treated rodents), 14 are identified to be *in vitro* OAT1 substrates. These 14 metabolites are predicted to be involved in clinically relevant DMIs with the 46 co-clustering drugs at the OAT1-level. A subset of 64 drug-metabolite pairs with similarity scores ≥0.250 (90% TS) was obtained (li_06_high_confidence_dmis.xlsx).

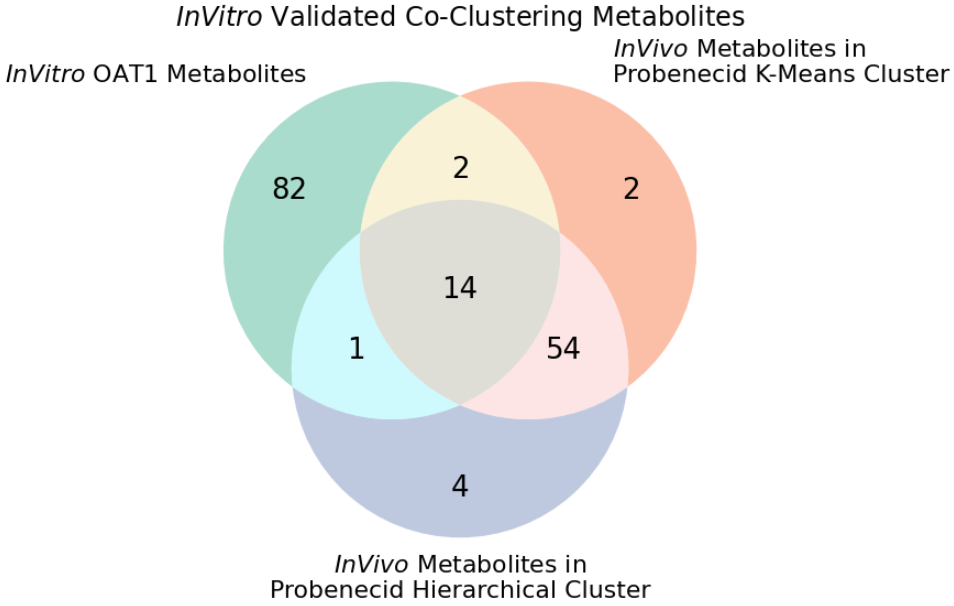

Figure 1. 4: Three-way Venn diagram. *In vitro* validated metabolites are at the intersection between all three circles. The overlapping area between the two *in vivo* metabolite sets represents the co-clustering metabolites.

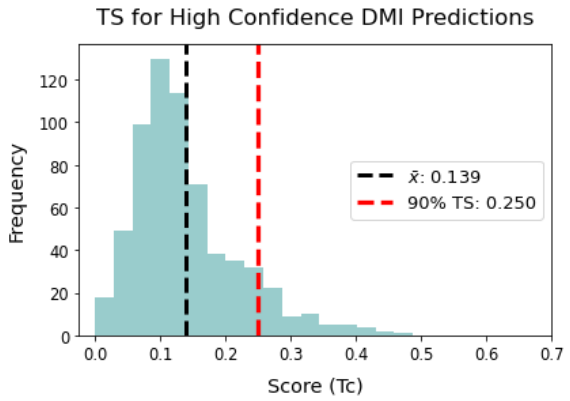

Figure 1. 5: Frequency distribution of similarity scores between drugs and metabolites. Black-dashed vertical line represents the mean score ($\bar{x}$). Red-dashed vertical line indicates the score at the 90th percentile (90% TS).

Table 1. 1: *In vitro* transporter kinetic parameters for co-clustering metabolites. Metabolites highlighted in yellow have high transport/inhibition affinities (<25 µM). *Proven *in vitro* inhibitors that don't have reported kinetics data. U/D, unpublished data from Nigam Lab.

Metabolite	Score	K_m (µM)	K_i (µM)	IC_{50} (µM)	Reference
4-Hydroxyphenyllactate	0.229		223		(Kaler et al., 2007)
Kynurenate	0.200		15	34 (5 6-CF)	(Bahn et al., 2005)
Kynurenine	0.197		1.4	12 (30 6-CF)	(Wikoff et al., 2011)
Xanthurenate	0.195		6	50 (30 6-CF)	(Wikoff et al., 2011)
Picolinate*	0.188				(Bahn et al., 2005)
Phenylalanine*	0.183				(Zalups & Ahmad, 2005)
Indolelactate	0.177			346 (6-CF)	U/D
Pyridoxate	0.149			2 (10 6-CF)	U/D
Serotonin	0.143			94 (10 6-CF)	U/D
Isoleucine*	0.141				(Zalups & Ahmad, 2005)
Glutarate	0.138	3.8	5.3	10.7 (4 6-CF)	(Bahn et al., 2005; Cihlar et al., 1999)
Leucine*	0.123				(Zalups & Ahmad, 2005)
3-Hydroxybutyrate	0.115		3220		(Kaler et al., 2007)
Cysteine*	0.097				(Zalups & Ahmad, 2005)

Inhibition of Fluorescent Tracer Uptake by Metabolite Compounds

The IC_{50} values for kynurenate (12.1 µM) and pyridoxate (2 µM) are similar to that of probenecid (3.9-7.7 µM). Based on *in vitro* data from literature, kynurenate, kynurenine, xanthurenate, pyridoxate and glutarate have with K_m or K_i/IC_{50} values <25 µM and are thus considered to be high affinity OAT1 substrates/inhibitors.

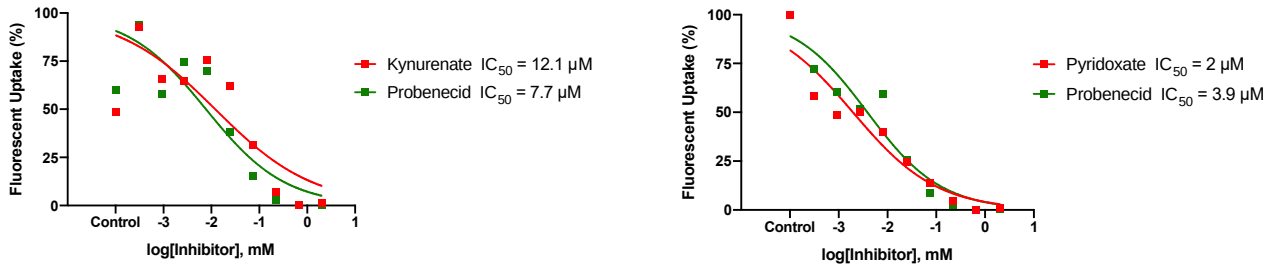

Figure 1. 6: Concentration-response curves for inhibition of fluorescence uptake via OAT1. Red data points indicate mean uptake for a given log[metabolite] in five same plate wells (n=5). Green data points represent mean uptake for a given log[probenecid] in three same plate wells (n=3).

Validate Clinical DDIs

Excluding the drugs that are unavailable in the US and therefore not accounted for by the Drug Interactions Checker tool (phenacetin, loxoprofen and pranoprofen) and mercaptopurine, 80% (33/41) of the probenecid-drug pairs are reported clinical DDIs attributed to the inhibition of renal secretion systems for organic small molecules and thus altered renal clearance. The mean pairwise similarity scores between probenecid and the FDA-approved co-clustering drugs and *in vitro* validated metabolites are equivalent (0.162). Notably, the median similarity score between the probenecid-metabolite pairs is greater than that of the probenecid-drug pairs (0.163 and 0.129, respectively).

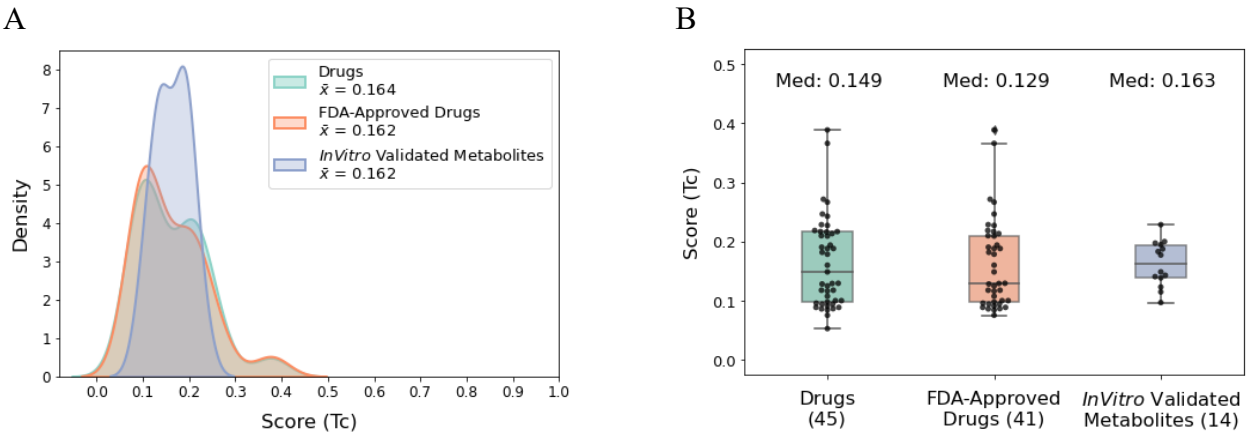

Figure 1. 7: Distribution of similarity scores between probenecid-compound pairs. (A) KDE plot shows the overall shape of the distribution/probability density. (B) Boxplot shows the minimum/maximum (upper/lower whiskers), first/third quartiles (width of the box) and median (center black line). Outliers are located outside of the whiskers.

Table 1. 2: Validation of predicted DDIs with probenecid. [1] and [2] indicate supporting data from the Drugs Interactions Checker tool by Drugs.com and Medscape, respectively. *Not FDA-approved.

Drug	Score	Reported	Reference
Tolbutamide	0.389	✓	[1], [2]
Chlorpropamide	0.366	✓	[1], [2]
Tolmetin	0.272	✓	
Sodium Benzoate	0.267	✓	[1]
Ibuprofen	0.247	✓	[1], [2]
Phenacetin*	0.243		
Aspirin	0.229	✓	[1], [2]
Acetaminophen	0.227	✓	[1]
Salicylate	0.219	✓	[1], [2]
Mefenamic Acid	0.217		
Loxoprofen*	0.217		
Betamipron*	0.216		
Furosemide	0.213		
Naproxen	0.210	✓	[1], [2]
Ketoprofen	0.209	✓	[1], [2]
4-Aminosalicylic Acid	0.194	✓	(Parvez et al., 2017)
Diflunisal	0.190	✓	[1], [2]
Flurbiprofen	0.188	✓	[1], [2]
Ethacrynic Acid	0.188	✓	[1]
Diclofenac	0.182	✓	[1], [2]
Melatonin	0.179		
Methazolamide	0.160		
Acetazolamide	0.149	✓	(Hasannejad et al., 2004)
Chlorothiazide	0.129	✓	[2]
Tazobactam	0.129		
Edaravone	0.128		
Cidofovir	0.125	✓	(Ho et al., 2000)
N-Acetylcysteine	0.118	✓	(Aslamkhan et al., 2003)
Stavudine	0.118		
Hydrochlorothiazide	0.116	✓	[1], [2]
Trichlormethiazide	0.108		
Cimetidine	0.100	✓	(Yanxiao et al., 2011)
Captopril	0.100	✓	[1], [2]
Adefovir	0.098	✓	(Maeda et al., 2014)
Tenofovir	0.096	✓	[2]
Zalcitabine	0.094	✓	[1]
Lamivudine	0.094	✓	[1]
Acyclovir	0.091	✓	[1], [2]
Theophylline	0.089		
Nicotine	0.089		
Caffeine	0.086	✓	[1]
Ganciclovir	0.086	✓	[1], [2]
Zidovudine	0.084	✓	[1], [2]
Didanosine	0.075	✓	(Takasawa et al., 1997)
Mercaptopurine	0.053		

2. OAT3

Summary

Here, we utilize two different input descriptor spaces and partitioning methods to obtain an optimized subset of structurally related molecules predicted to compete for the same substrate binding site of OAT3. The chemical dataset of 226 compounds (117 *in vivo* metabolites and 109 *in vitro* drug substrates) is decomposed to a subset of 10 metabolites and 38 drugs that are predicted to competitively compete for OAT3 transport at the level of competitive binding. We identify the following OAT3-mediated metabolic pathways affected by DMIs: Cys and Trp metabolism, fatty acid metabolism, vitamin B6 metabolism and pyrimidine metabolism. Kynurenate and cysteine are prototype protein-bound uremic toxins predicted to have their levels elevated in the plasma due to competition for OAT3-mediated renal elimination. The competing drug compounds belong to the following therapeutic classes: analgesics, antibiotics, NSAIDs, antacids, renal protectants, uricosurics, antihypertensives, chemotherapeutics, antivirals and diuretics. We predict that the administration of one or a combination of these drugs can potentially cause metabolic alterations (of all these metabolites) and unexpected side effects in patients. 38 drug-metabolite pairs are highly predicted to compete for the same substrate binding site of OAT3. These high confidence DMI predictions can be experimentally validated via *in vitro* uptake assays, as discussed further below.

Decomposition Step 1: K-Means Clustering

Figure 2.1 shows that the first 14 PCs explain 90.2% of the variance and are thus retained in the transformed compound dataset. The mean silhouette plot shows k=3 and k=4 to have equivalent scores (0.256 and 0.255, respectively). The silhouette plots in Figure 2.2B indicate the following: the clusters are relatively homogenous in size and the probenecid cluster has a

majority of its instances with silhouette scores greater than the mean, all of which are non-negative values, thereby indicating correct cluster assignments.

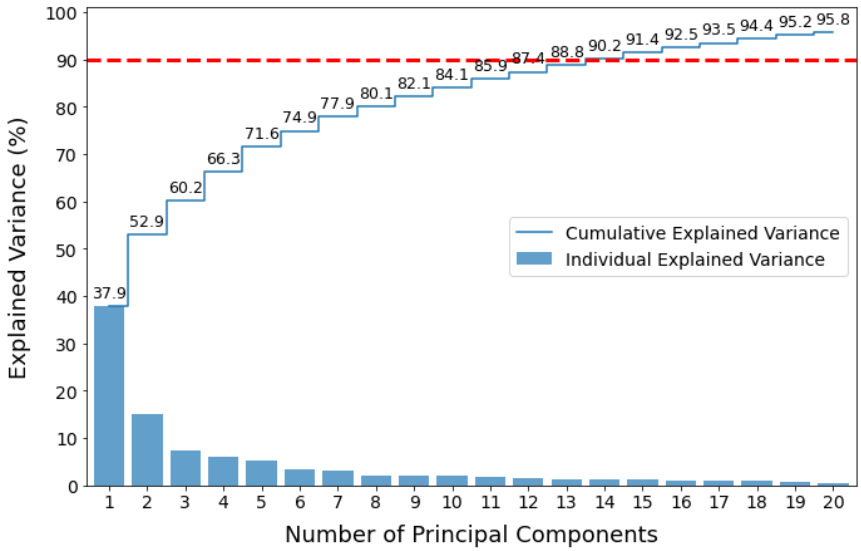

Figure 2. 1: PCA scree plot. Bar graph with individual explained variance and step chart with cumulative explained variance vs. principal components. Red-dashed line represents the 90% cumulative variance threshold.

The elbow plot shows the elbow to be located between k=3 and k=4. The Davis-Bouldin score plot denotes better inter-cluster separation and intra-cluster homogeneity for k=4 compared to that of k=3, given their respective DB indexes 1.41 and 1.58 (Figure 2.2D). The three internal evaluation methods are in agreement that k=4 is optimal for K-Means clustering; when k=4, the compound dataset is partitioned such that the resulting clusters that are distinct, dense and homogenous cluster. The compound dataset is decomposed to a subset of 112 structurally related molecules based on 1D molecular descriptors. 70 endogenous metabolites and 38 drugs, including probenecid, are recovered from cluster 3. The remaining 50% (112/226) of the chemical dataset is discarded.

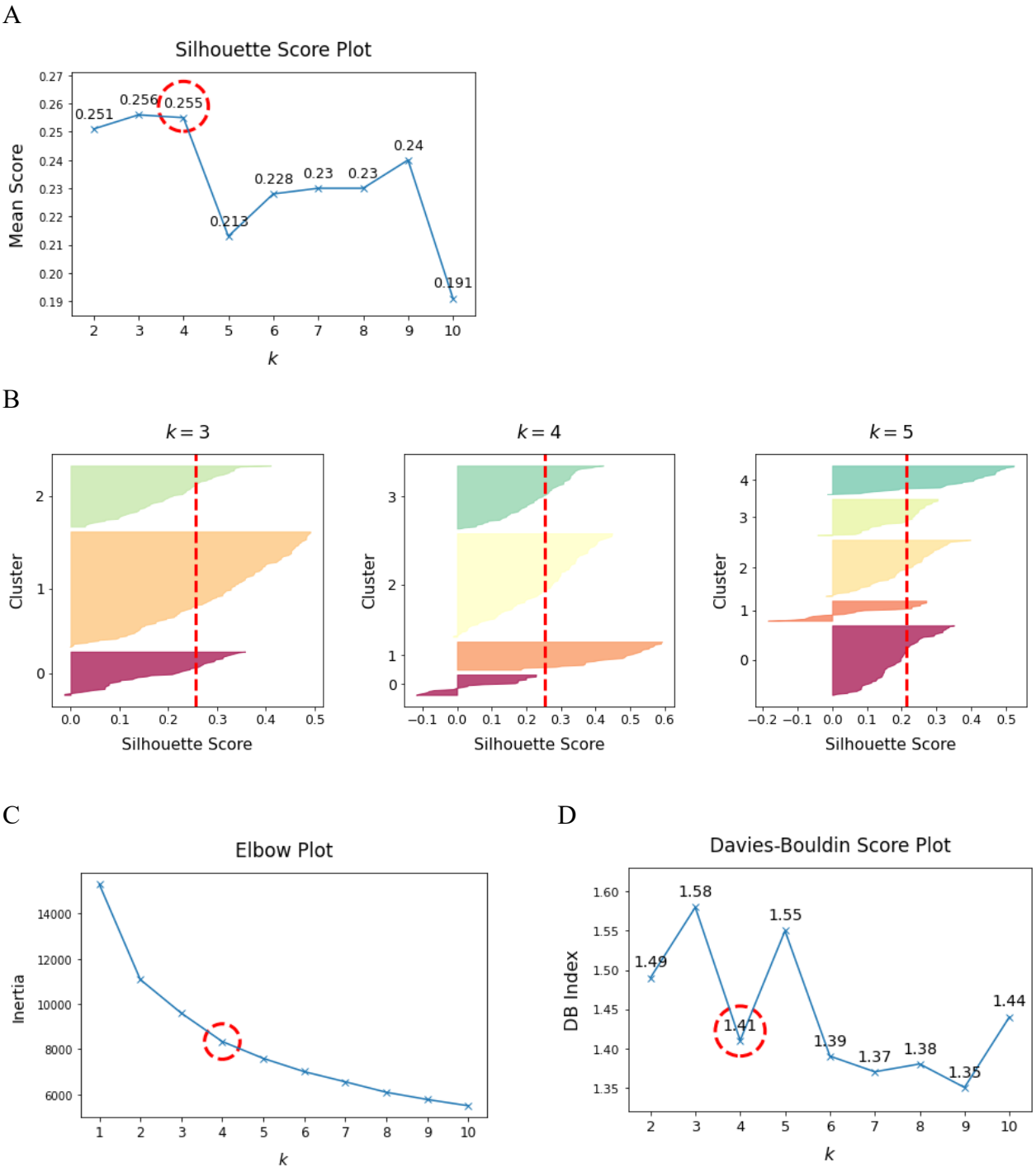

Figure 2. 2: Evaluation results on the internal evaluation of `KMeans`. The optimal score for each parameter – (A) silhouette, (C) elbow or (D) Davies-Bouldin – is circled in red. (B) Height of the silhouette plot indicates cluster size. Widths correspond to individual silhouette scores. Red-dashed vertical lines represent mean silhouette scores.

Decomposition Step 2: Hierarchical Agglomerative Clustering

Average linkage has the highest CCC (0.869) and thus preserves the "ground truth" similarities between molecules the best (li_05_ccc_outputs.xlsx). The dendrogram tree denotes large vertical distances between the first two cluster splits and the next two splits (0.39 and 0.36, respectively). At these distance thresholds, we obtain two and three clusters, respectively, with maximized inter-cluster dissimilarities. The maximum absolute second derivative is at k=3. Thus, a cut-off distance of d=2.2 was set to partition the chemical dataset into three optimal clusters based on Morgan FPs. 73 endogenous metabolites and 106 drugs, including probenecid, are recovered from cluster 1. The remaining 21% (47/226) of the chemical dataset is discarded.

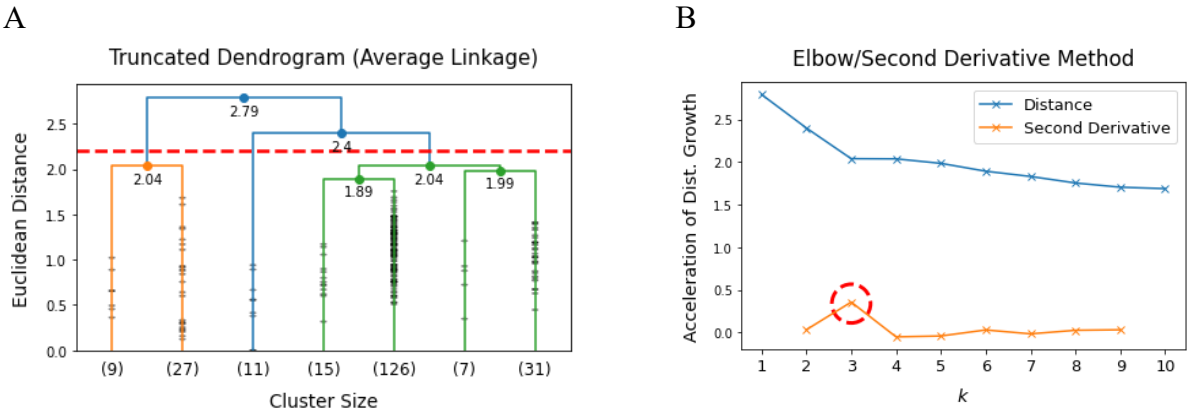

Figure 2. 3: Average linkage hierarchical clustering results. Red-dashed line indicates the cut-off distance. Red circle represents the maximum absolute second derivative, which corresponds to the elbow on the blue curve. (B) Second derivative values measure the rates at which the distances between clustering steps change.

Decomposition Step 3: Co-Clustering Method

67 metabolites and 38 drugs overlap between the probenecid-containing K-Means and hierarchical clusters. As such, the co-clustering method further decomposes the chemical dataset to a subset of 105 compounds that have been optimized for molecular similarity using two different input molecule descriptors and clustering algorithms.

OAT3-Mediated DMI Predictions

Out of the 67 co-clustering *in vivo* metabolites, 10 are identified to be *in vitro* OAT3 substrates. These 10 metabolites are predicted to be involved in clinically relevant DMIs with the 38 co-clustering drugs at the OAT3-level. A subset of 38 drug-metabolite pairs with similarity scores ≥0.237 (90% TS) was obtained (li_06_high_confidence_dmis.xlsx).

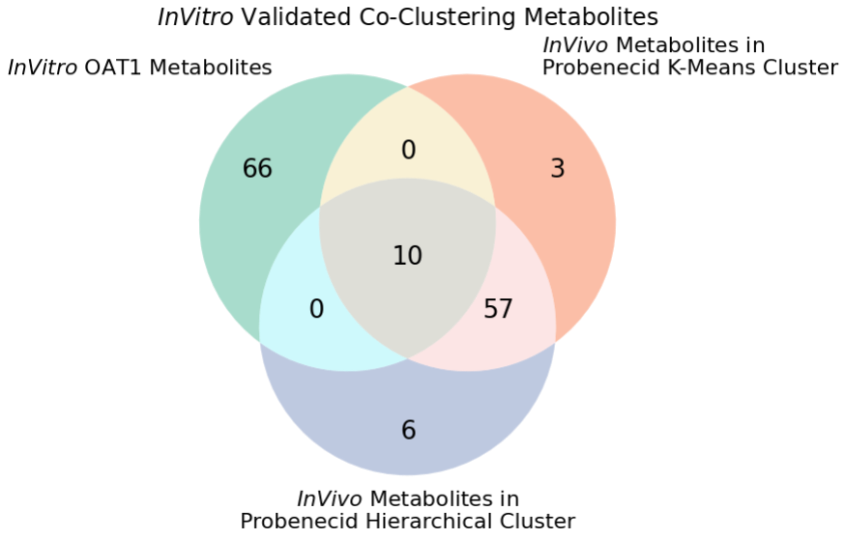

Figure 2. 4: Three-way Venn diagram. *In vitro* validated metabolites are at the intersection between all three circles. The overlapping area between the two *in vivo* metabolite sets represents the co-clustering metabolites.

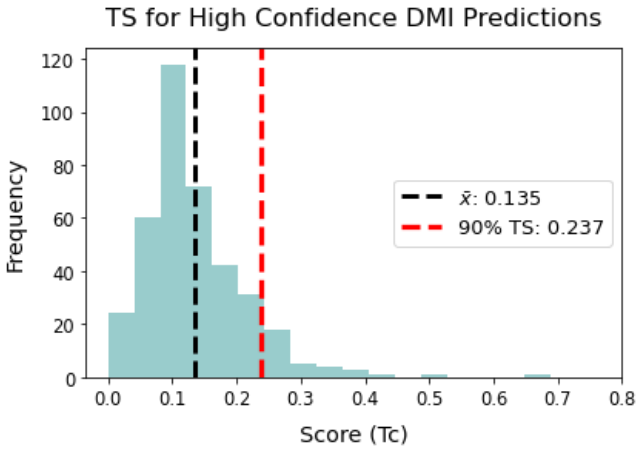

Figure 2. 5: Frequency distribution of similarity scores between drugs and metabolites. Black-dashed vertical line represents the mean score ($\bar{x}$). Red-dashed vertical line indicates the score at the 90th percentile (90% TS).

Table 2. 1: *In vitro* transporter kinetic parameters for co-clustering metabolites. Metabolites highlighted in yellow have high transport/inhibition affinities (<25 µM). *Proven *in vitro* inhibitors that don't have reported kinetics data. U/D, unpublished data from Nigam Lab.

Metabolite	Score	K_m (µM)	K_i (µM)	IC_{50} (µM)	Reference
Kynurenate	0.200		5.5	8 (5 6-CF)	(Bahn et al., 2005)
Xanthurenate	0.195		7.9	11.5 (5 6-CF)	(Bahn et al., 2005)
Picolinate*	0.188				(Bahn et al., 2005)
Indolelactate	0.177			67 (10 5-CF)	U/D
Pyridoxate	0.149			5 (10 5-CF)	U/D
Serotonin	0.143			193 (10 5-CF)	U/D
Glutarate	0.138	23			(Bahn et al., 2005)
Malonate*	0.115				(Anzai et al., 2005)
Cysteine*	0.097				(Bahn et al., 2005)
Thymidine	0.090		338	384 (50 5-CF)	(Vallon et al., 2008)

Inhibition of Fluorescent Tracer Uptake by Metabolite Compounds

The IC_{50} of pyridoxate (5 µM) is comparable to that of probenecid (1.6-2.2 µM) while the IC_{50} of indolelactate (67 µM) is larger than that of probenecid. Based on literature data, kynurenate, xanthurenate, pyridoxate and glutarate have K_m or K_i/IC_{50} values <25 µM and are thus considered to be high affinity OAT3 substrate/inhibitors (Table 2.1).

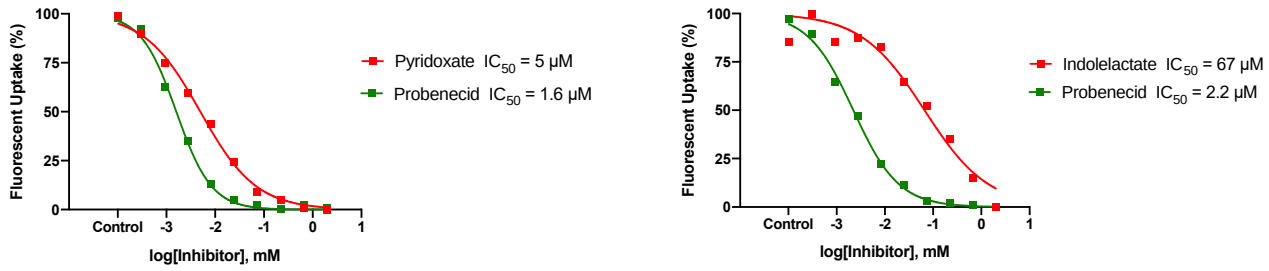

Figure 2. 6: Concentration-response curves for inhibition of fluorescence uptake via OAT3. Red data points indicate mean uptake for a given log[metabolite] in five same plate wells (n=5). Green data points represent mean uptake for a given log[probenecid] in three same plate wells (n=3).

Validate Clinical DDIs

Excluding the drugs that are not FDA-approved and therefore not accounted for by the Drug Interactions Checker tool (phenacetin, loxoprofen, betamipron and pranoprofen) and mercaptopurine, two-thirds (21/32) of the probenecid-drug pairs are reported clinical DDIs attributed to the inhibition of renal secretion systems for organic small molecules and thus altered renal clearance. The mean and median pairwise similarity scores between probenecid and the FDA-approved co-clustering drugs (0.154 and 0.139, respectively) are comparable to those of the *in vitro* validated metabolites (0.149 and 0.146, respectively).

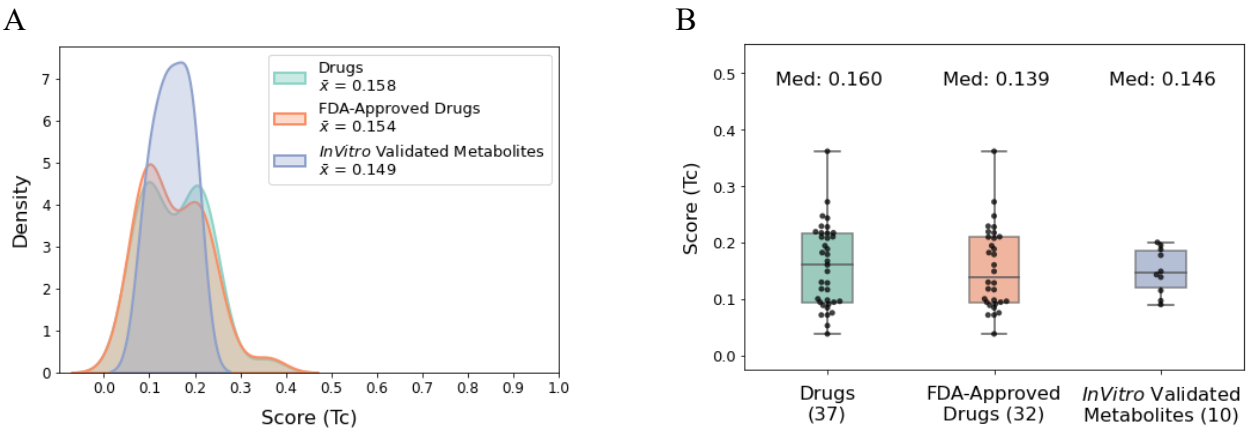

Figure 2. 7: Distribution of pairwise similarity scores between probenecid and co-clustering compounds. (A) KDE plot shows the overall shape of the distribution/probability density. (B) Boxplot shows the minimum/maximum (upper/lower whiskers), first/third quartiles (width of the box) and median (center black line). Outliers are located outside of the whiskers.

Table 2. 2: Validation of predicted DDIs with probenecid. [1] and [2] indicate supporting data from the Drugs Interactions Checker tool by Drugs.com and Medscape, respectively. *Not FDA-approved.

Drug	Score	Reported	Reference
Procainamide	0.361		
Tolmetin	0.272	✓	[1], [2]
Ibuprofen	0.247	✓	[1], [2]
Phenacetin*	0.243		
Aspirin	0.229	✓	[1], [2]
Acetaminophen	0.227	✓	[1]
Salicylate	0.219	✓	[1], [2]
Mefenamic Acid	0.217		
Loxoprofen*	0.217		
Betamipron*	0.216		
Naproxen	0.210	✓	[1], [2]
Ketoprofen	0.209	✓	[1], [2]
Gemfibrozil	0.207		
4-Aminosalicylic Acid	0.194	✓	(Parvez et al., 2017)
Ethacrynic Acid	0.188	✓	[1]
Diclofenac	0.182	✓	[1], [2]
Melatonin	0.179		
Pranoprofen*	0.167		
Methazolamide	0.160		
Acetazolamide	0.149		
Chlorothiazide	0.129	✓	[2]
Edaravone	0.128		
Stavudine	0.118		
Hydrochlorothiazide	0.116	✓	[1], [2]
Cimetidine	0.100	✓	(Yanxiao et al., 2011)
Adefovir	0.098	✓	(Maeda et al., 2014)
Tenofovir	0.096	✓	[2]
Zalcitabine	0.094	✓	[1]
Lamivudine	0.094	✓	[1]
Acyclovir	0.091	✓	[1], [2]
Nicotine	0.089		
Zidovudine	0.084	✓	[1], [2]
Didanosine	0.075	✓	(Takasawa et al., 1997)
Azathioprine	0.071	✓	(Watanabe & Nagashima, 1983)
Fluorouracil	0.071		
Mercaptopurine	0.053		
Thioguanine	0.038		

DISCUSSION

Applicability of Deterministic Model for Predicting Clinically Relevant DMIs

The Drug Interactions Checker tool and literature data were used to validate the OAT-mediated DDI predictions between probenecid and the co-clustering drugs. Due to the limited available *in vitro*/clinical data for drug-metabolite interactions, we compared similarity scores between the probenecid-drug pairs and probenecid-metabolite pairs to assess the applicability of our proposed multi-step model for predicting clinically relevant OAT-mediated DMIs.

33/41 (80%) of the predicted OAT1-mediated probenecid-drug interactions are reported clinical DDIs attributed to altered renal clearance presumably due to inhibition of renal secretion systems for organic small molecules. Given the comparable mean and median similarity scores between probenecid and the 14 *in vitro* validated metabolites (0.162 and 0.163, respectively) and 41 FDA-approved drugs (0.162 and 0.129, respectively), as well as the high predictive accuracy of clinical DDIs (≥80%), we demonstrate the applicability of the proposed deterministic model for accurately predicting clinically relevant OAT1-mediated DMIs.

While 80% of the predicted probenecid-drug interactions are validated to be clinically relevant, many don't have high structural similarity to probenecid and have pairwise similarity scores as low as 0.075 (Table 1.2). The high predictive accuracy of our proposed multi-step model can be attributed to the utilization of a consensus approach that captures relevant information and useful intermolecular relationships from different input descriptor spaces and clustering methods, respectively, to define a chemical space with optimized molecular similarity that is more useful for DMI predictions.

The 1D descriptor spaces and 2D fingerprint spaces capture different aspects of the chemical structure and so recovers different drugs and metabolites in each space. The multi-step

decomposition problem is to create partitions of the interaction edges (drug-drug, drug-metabolite and metabolite-metabolite interactions) such that intra-cluster homogeneity and inter-cluster dissimilarity are maximized. Indeed, the unsupervised K-Means and hierarchical clustering methods are useful in the retrieval of structurally related subsets of molecules from which drug-metabolite interactions can be predicted. By the described consensus approach, the overlapping (common) chemical spaces in which drugs and metabolites exhibit high similarity levels are predicted to infer similar physiological effects and compete for the same substrate binding site at the OAT1-level.

21/32 (Two-thirds) of the predicted OAT3-mediated probenecid-drug interactions are reported clinical DDIs attributed to the inhibition of renal secretion systems for organic small molecules and altered renal clearance. Given the comparable mean and median similarity scores between probenecid and the 10 *in vitro* validated metabolites (0.149 and 0.146, respectively) and 32 FDA-approved co-clustering drugs (0.154 and 0.139, respectively), as well as the moderate predictive accuracy for clinical DDIs (≥66%), we demonstrate the applicability of the proposed deterministic model for accurately predicting clinically relevant DMIs at the OAT3-level. Although the predictive accuracy isn't as robust as that of the OAT1-mediated DDIs, our quantitative analyses provide insight into the role of renal uptake transporters in unexplained drug side effects and secondary (indirect) effects of DMIs in the context of drug-induced metabolic alterations and disease states (e.g., CKD, metabolic syndrome, diabetes).

Future Directions: In Vitro/Clinical Validation of Predicted DMIs

Our DMI predictions can be experimentally validated via *in vitro* uptake assays in cells stably overexpressing the renal transporter using a radiolabeled metabolite compound to monitor the uptake activity of the transporter at various concentrations. Results from the uptake assays in

the presence and absence of a drug compound at a fixed concentration would determine whether the tested drug-metabolite pair competes for transport at the level of competitive binding. *In vivo* metabolomics in drug-treated humans would also help establish drug-metabolite interactions as something that should be considered in drug dosing and safety.

Clinical Implications of Transporter-Mediated DMIs

Another important aspect of drug-metabolite interactions is that some of these compounds can be utilized as endogenous biomarkers for novel drug entities. Here, we highlight another practical application of the proposed model. In fact, pyridoxate has been recently identified as a sensitive endogenous biomarker for OAT1/OAT3 inhibition in animal models (Shen et al., 2018). A selective endogenous biomarker whose levels are not dependent upon food intake or diurnal rhythms can be very useful for *in vivo* analysis of novel drug entities. Furthermore, in the case of CKD, the loss of renal function is the combined effect of glomerular and tubular damage. Recent research has focused on identifying specific biomarkers for tubular function, and several of the endogenous metabolites here may have some application as clinical biomarkers.

The consequences of drug-metabolite interactions have yet to be fully explored. However, it is possible that even slight increases in concentration can have major consequences on metabolic signaling pathways in organs. Based on preliminary data following probenecid administration in rodent models, it appears that the levels of multiple metabolites are altered (S. K. Nigam et al., 2015). By understanding the patterns of metabolic dysregulation, we can also determine the homeostatic mechanisms that return the body to normal.

While not explored in this work, it is also likely that there are intracellular consequences due to drug-metabolite interactions. Altering levels of metabolites can impact a wide range of

downstream processes, from energy metabolism to cellular signaling and gene expression across multiple tissues. For example, bile acids act as signaling molecules that activate FXR (farsenoid X receptor) and GPBAR1 (G protein-coupled bile acid receptor 1; TGR5) to regulate bile acid concentrations in the liver, intestine and blood via a negative feedback mechanism. FXR and TGR5 thus act as metabolic sensors that directly regulate the enterohepatic circulation of bile acids via induction of FXR-dependent genes and activation of downstream cellular signaling pathways in multiple tissues, including liver, intestine, kidney, skeletal muscles, pancreas, adipocytes, macrophages, spleen and gallbladder (Chiang, 2013). They regulate gene expression levels of several brush border membrane transporters to mediate bile acid uptake in the liver, reabsorption and secretion in the intestine and renal elimination in the urine. Renal uptake transporters, OAT3 in particular, play a central role in mediating the flow of bile acids through the gut-liver-kidney axis and renal elimination of bile acids. Thus, accumulated plasma levels of bile acids as a result of OAT3 inhibition by drugs (i.e., competition for renal uptake) can cause an overload of cellular bile acids in the liver and intestine and upregulation of several FXR- and TGR5-dependent genes in multiple tissues. FXR and TGR5 not only mediate bile acid sensing for bile acid and cholesterol metabolism, they also regulate glucose and lipid homeostasis (Claudel et al., 2005), underscoring the indirect effects of drug-induced metabolic alterations on the endogenous role of drug transporters in regulating local and systemic homeostasis. More studies are needed to understand the mechanistic interplay between transporters and metabolic sensors in metabolic signaling. However, we provide a potential link between renal drug transporters and metabolic regulation in the context of drug-metabolite interactions.

Another example of secondary adverse effects of drug-metabolite interactions is the overactivation of transcription factor aryl hydrocarbon receptor (AHR) by tryptophan-derived

uremic toxins (e.g., indoxyl sulfate, indoleacetate, kynurenine) accumulated in the plasma. Increased exposure to AHR-activating ligands, several of which are OAT1 and OAT3 substrates, may cause upregulation of several AHR-regulated genes and induction of reactive oxygen species production via downstream cellular signaling pathways across multiple epithelial tissues, resulting in systemic inflammatory responses (Sallée et al., 2014).

Here, we present a novel way of analyzing the endogenous role of drug transporters. While we are limited by the amount of high-quality *in vivo* data available for specific drug transporters (OATP1B1/OATP1B3 in the liver, for example), we have developed an adaptable multi-step workflow that can be applied to proteins with multiple substrates. Currently, we have focused on a subset of clinically relevant renal drug transporters, but future directions may apply this approach to other tissue-specific transporter proteins as well as drug-metabolizing enzymes and nuclear receptors.

BIBLIOGRAPHY

Anzai, N., Jutabha, P., Enomoto, A., Yokoyama, H., Nonoguchi, H., Hirata, T., Shiraya, K., He, X., Seok, H. C., Takeda, M., Miyazaki, H., Sakata, T., Tomita, K., Igarashi, T., Kanai, Y., & Endou, H. (2005). Functional characterization of rat organic anion transporter 5 (Slc22a19) at the apical membrane of renal proximal tubules. *Journal of Pharmacology and Experimental Therapeutics*, *315*(2), 534–544. https://doi.org/10.1124/jpet.105.088583

Aslamkhan, A. G., Han, Y. H., Yang, X. P., Zalups, R. K., & Pritchard, J. B. (2003). Human renal organic anion transporter 1-dependent uptake and toxicity of mercuric-thiol conjugates in madin-darby canine kidney cells. *Molecular Pharmacology*, *63*(3), 590–596. https://doi.org/10.1124/mol.63.3.590

Bahn, A., Ljubojević, M., Lorenz, H., Schultz, C., Ghebremedhin, E., Ugele, B., Sabolić, I., Burckhardt, G., & Hagos, Y. (2005). Murine renal organic anion transporters mOAT1 and mOAT3 facilitate the transport of neuroactive tryptophan metabolites. *American Journal of Physiology - Cell Physiology*, *289*(5 58-5). https://doi.org/10.1152/ajpcell.00619.2004

Bush, K. T., Wu, W., Lun, C., & Nigam, S. K. (2017). The drug transporter OAT3 (SLC22A8) and endogenous metabolite communication via the gut–liver– kidney axis. *Journal of Biological Chemistry*, *292*(38), 15789–15803. https://doi.org/10.1074/jbc.M117.796516

Chiang, J. Y. L. (2013). Bile acid metabolism and signaling. *Comprehensive Physiology*, *3*(3), 1191–1212. https://doi.org/10.1002/cphy.c120023

Cihlar, T., Lin, D. C., Pritchard, J. B., Fuller, M. D., Mendel, D. B., & Sweet, D. H. (1999). The antiviral nucleotide analogs cidofovir and adefovir are novel substrates for human and rat renal organic anion transporter 1. *Molecular Pharmacology*, *56*(3), 570–580. https://doi.org/10.1124/mol.56.3.570

Claudel, T., Staels, B., & Kuipers, F. (2005). The Farnesoid X receptor: A molecular link between bile acid and lipid and glucose metabolism. In *Arteriosclerosis, Thrombosis, and Vascular Biology* (Vol. 25, Issue 10, pp. 2020–2031). Lippincott Williams & Wilkins. https://doi.org/10.1161/01.ATV.0000178994.21828.a7

Giacomini, K. M., Huang, S. M., Tweedie, D. J., Benet, L. Z., Brouwer, K. L. R., Chu, X., Dahlin, A., Evers, R., Fischer, V., Hillgren, K. M., Hoffmaster, K. A., Ishikawa, T., Keppler, D., Kim, R. B., Lee, C. A., Niemi, M., Polli, J. W., Sugiyama, Y., Swaan, P. W., … Zhang, L. (2010). Membrane transporters in drug development. In *Nature Reviews Drug Discovery* (Vol. 9, Issue 3, pp. 215–236). https://doi.org/10.1038/nrd3028

Hasannejad, H., Takeda, M., Taki, K., Shin, H. J., Babu, E., Jutabha, P., Khamdang, S., Aleboyeh, M., Onozato, M. L., Tojo, A., Enomoto, A., Anzai, N., Narikawa, S., Huang, X. L., Niwa, T., & Endou, H. (2004). Interactions of Human Organic Anion Transporters with Diuretics. *Journal of Pharmacology and Experimental Therapeutics*, *308*(3), 1021–1029. https://doi.org/10.1124/jpet.103.059139

Ho, E. S., Lin, D. C., Mendel, D. B., & Cihlar, T. (2000). *Cytotoxicity of Antiviral Nucleotides Adefovir and Cidofovir Is Induced by the Expression of Human Renal Organic Anion Transporter 1*.

Hörl, W. H. (2010). Nonsteroidal anti-inflammatory drugs and the kidney. In *Pharmaceuticals* (Vol. 3, Issue 7, pp. 2291–2321). MDPI AG. https://doi.org/10.3390/ph3072291

Iwaki, M., Shimada, H., Irino, Y., Take, M., & Egashira, S. (2017). Inhibition of methotrexate uptake via organic anion transporters OAT1 and OAT3 by glucuronides of nonsteroidal anti-inflammatory drugs. *Biological and Pharmaceutical Bulletin*, *40*(6), 926–931. https://doi.org/10.1248/bpb.b16-00970

Kaler, G., Truong, D. M., Khandelwal, A., Nagle, M., Eraly, S. A., Swaan, P. W., & Nigam, S. K. (2007). Structural variation governs substrate specificity for Organic Anion Transporter (OAT) homologs: Potential remote sensing by OAT family members. *Journal of Biological Chemistry*, *282*(33), 23841–23853. https://doi.org/10.1074/jbc.M703467200

Kaminski, T. W., Pawlak, K., Karbowska, M., Znorko, B., Mor, A. L., Mysliwiec, M., & Pawlak, D. (2019). The impact of antihypertensive pharmacotherapy on interplay between protein-bound uremic toxin (indoxyl sulfate) and markers of inflammation in patients with chronic kidney disease. *International Urology and Nephrology*, *51*(3), 491–502. https://doi.org/10.1007/s11255-018-02064-3

Maeda, K., Tian, Y., Fujita, T., Ikeda, Y., Kumagai, Y., Kondo, T., Tanabe, K., Nakayama, H., Horita, S., Kusuhara, H., & Sugiyama, Y. (2014). Inhibitory effects of p-aminohippurate and probenecid on the renal clearance of adefovir and benzylpenicillin as probe drugs for organic anion transporter (OAT) 1 and OAT3 in humans. *European Journal of Pharmaceutical Sciences*, *59*(1), 94–103. https://doi.org/10.1016/j.ejps.2014.04.004

Nigam, A. K., Li, J. G., Lall, K., Shi, D., Bush, K. T., Bhatnagar, V., Abagyan, R., & Nigam, S. K. (2020). *Unique metabolite preferences of the drug transporters OAT1 and OAT3 analyzed by machine learning Downloaded from*. https://doi.org/10.1074/jbc.RA119.010729

Nigam, S. K. (2014). What do drug transporters really do? In *Nature Reviews Drug Discovery* (Vol. 14, Issue 1, pp. 29–44). Nature Publishing Group. https://doi.org/10.1038/nrd4461

Nigam, S. K., Bush, K. T., Martovetsky, G., Ahn, S. Y., Liu, H. C., Richard, E., Bhatnagar, V., & Wu, W. (2015). The organic anion transporter (OAT) family: A systems biology perspective. *Physiological Reviews*, *95*(1), 83–123. https://doi.org/10.1152/physrev.00025.2013

Parvez, M. M., Shin, H. J., Jung, J. A., & Shin, J. G. (2017). Evaluation of para-aminosalicylic acid as a substrate of multiple solute carrier uptake transporters and possible drug interactions with nonsteroidal antiinflammatory drugs in vitro. *Antimicrobial Agents and Chemotherapy*, *61*(5). https://doi.org/10.1128/AAC.02392-16

Roth, M., Obaidat, A., & Hagenbuch, B. (2012). OATPs, OATs and OCTs: The organic anion and cation transporters of the SLCO and SLC22A gene superfamilies. *British Journal of Pharmacology*, *165*(5), 1260–1287. https://doi.org/10.1111/j.1476-5381.2011.01724.x

Sallée, M., Dou, L., Cerini, C., Poitevin, S., Brunet, P., & Burtey, S. (2014). The aryl hydrocarbon receptor-activating effect of uremic toxins from tryptophan metabolism: A new concept to understand cardiovascular complications of chronic kidney disease. In *Toxins* (Vol. 6, Issue 3, pp. 934–949). Multidisciplinary Digital Publishing Institute (MDPI). https://doi.org/10.3390/toxins6030934

Shen, H., Nelson, D. M., Oliveira, R. V., Zhang, Y., McNaney, C. A., Gu, X., Chen, W., Su, C., Reily, M. D., Shipkova, P. A., Gan, J., Lai, Y., Marathe, P., & Humphreys, W. G. (2018). Discovery and validation of pyridoxic acid and homovanillic acid as novel endogenous plasma biomarkers of organic anion transporter (OAT) 1 and OAT3 in Cynomolgus monkeys. *Drug Metabolism and Disposition*, *46*(2), 178–188. https://doi.org/10.1124/dmd.117.077586

Takasawa, K., Terasaki, T., Suzuki, H., & Sugiyama, Y. (1997). *In Vivo Evidence for Carrier-Mediated Efflux Transport of 3-Azido-3-Deoxythymidine and 2,3-Dideoxyinosine Across the Blood-Brain Barrier via a Probenecid-Sensitive Transport System 1*.

Vallon, V., Eraly, S. A., Wikoff, W. R., Rieg, T., Kaler, G., Truong, D. M., Ahn, S. Y., Mahapatra, N. R., Mahata, S. K., Gangoiti, J. A., Wu, W., Barshop, B. A., Siuzdak, G., & Nigam, S. K. (2008). Organic anion transporter 3 contributes to the regulation of blood pressure. *Journal of the American Society of Nephrology*, *19*(9), 1732–1740. https://doi.org/10.1681/ASN.2008020180

Watanabe, A., & Nagashima, H. (1983). Glutathione metabolism and glucose 6-phosphate dehydrogenase activity in experimental liver injury. *Acta Medica Okayama*, *37*(6), 463–470. https://doi.org/10.18926/AMO/32401

Wikoff, W. R., Nagle, M. A., Kouznetsova, V. L., Tsigelny, I. F., & Nigam, S. K. (2011). Untargeted metabolomics identifies enterobiome metabolites and putative uremic toxins as substrates of organic anion transporter 1 (Oat1). *Journal of Proteome Research*, *10*(6), 2842–2851. https://doi.org/10.1021/pr200093w

Wu, W., Bush, K. T., & Nigam, S. K. (2017). Key Role for the Organic Anion Transporters, OAT1 and OAT3, in the in vivo Handling of Uremic Toxins and Solutes. *Scientific Reports*, *7*(1). https://doi.org/10.1038/s41598-017-04949-2

Yanxiao, C., Ruijuan, X., Jin, Y., Lei, C., Qian, W., Xuefen, Y., Hong, T., Xueying, Z., Davey, A. K., & Jiping, W. (2011). Organic anion and cation transporters are possibly involved in renal excretion of entecavir in rats. *Life Sciences*, *89*(1–2), 1–6. https://doi.org/10.1016/j.lfs.2011.03.018

Yu, C. P., Sweet, D. H., Peng, Y. H., Hsieh, Y. W., Chao, P. D. L., Hou, Y. C., & Lin, S. P. (2017). Effects of nonsteroidal anti-inflammatory drugs on the renal excretion of indoxyl sulfate, a nephro-cardiovascular toxin, in rats. *European Journal of Pharmaceutical Sciences*, *101*, 66–70. https://doi.org/10.1016/j.ejps.2017.02.007

Zalups, R. K., & Ahmad, S. (2005). Transport of N-acetylcysteine S-conjugates of methylmercury in Madin-Darby canine kidney cells stably transfected with human isoform of organic anion transporter 1. *Journal of Pharmacology and Experimental Therapeutics*, *314*(3), 1158–1168. https://doi.org/10.1124/jpet.105.086645